TRIBO-CORROSION BEHAVIOUR OF TiC_xO_y THIN FILMS IN BIO-FLUIDS

M.T. Mathew [1,2], E. Ariza [1], L. A. Rocha [1,3], F. Vaz [4], A.C. Fernandes [4], M .M. Stack [5]

[1] Centre for Mechanics and Materials Technologies (CT2M), Universidade do Minho, Azurém, 4800-058 Guimarães, Portugal.

[2] Tribology group, Department of Orthopaedic Surgery, Rush University Medical Centre (RUMC), 1653 W. Congress Pkwy, Chicago, IL60612, USA

[3] Universidade do Minho, Dept. Eng. Mecânica, Azurém, 4800-058 Guimarães, Portugal

[4] Universidade do Minho, Dept. Física, Azurém, 4800-058 Guimarães, Portugal.

[5] Dept. Mechanical Engineering, University of Strathclyde, James Weir Building, 75 Montrose Street, Glasgow, G1 2XJ, UK

Abstract:

In recent years, the development of thin film systems for decorative applications has attracted significant attention in scientific research. These decorative coatings require, not only an attractive appearance for market applications, but also an ability to protect the surface underneath. Because of this, corrosion, wear and their combined effects (termed tribo-corrosion) are particularly important for lifetime prediction.

The tribo-corrosion behaviour of a range of single layered titanium oxycarbide, TiC_xO_y,coatings, produced by DC reactive magnetron sputtering, has been studied and reported as a function of electrode potential (-0.9 V, -0.5 V, 0.0 V and +0.5 V) and applied load (3, 6 and 9 N). The study was conducted in a reciprocating sliding tribo-system (Plint TE 67/E) in a bio fluid (an artificial perspiration solution) at room temperature. During the wear tests, both the open-circuit potential and the corrosion current were monitored.

The results showed that electrode potential and load have a significant influence on the total material loss. The variations in R_p (polarization resistance) and C_f (capacitance) before and after sliding, obtained by Electrochemical Impedance Spectroscopy (EIS) were evaluated in order to provide an understanding of the resistance of the film in such conditions. Tribo-corrosion maps were generated, based on the results, indicating the change in mechanisms of the tribological and corrosion parameters for such coatings.

Key words: Tribo-Corrosion, Applied load, Electrode potential, Electrochemical Impedance Spectroscopy (EIS), Synergism.

1. Introduction

Surface coatings need to be resistant to wear and corrosion and have an attractive appearance and coloration. To satisfy such requirements, among the available surface coating methods, plasma-based PVD techniques are significant due to the flexibility and range of options available in manufacturing such films [1-2]. The high chemical stability, surface mechanical resistance and adhesion to the decorative components are some of the main attractive qualities that are associated with PVD technologies [3-4]. Among the number of available thin film materials/systems, metal-based oxy carbides, and in particular titanium oxycarbides, TiC_xO_y are becoming very popular due to their superior mechanical properties (hardness, adhesion, moderate level of compressive residual stresses, etc.) and chemical and tribological properties (essentially corrosion and wear) and potentially attractive colourations (several shades of grey and tones of gold, brown and dark blue/blacks) [5-6]. These are candidate coatings for door handles, spectacle frames and other household components [1].

During every day usage, such components are exposed to rubbing or sliding, in the presence of particles and chemical solutions, for example, perspiration. Thus far, research on these decorative thin film systems has often focused on the possibility to change the film coloration by varying deposition parameters (target materials, gaseous atmospheres, bias voltage usage, temperature, etc.). Only recently has work been carried out to study the coated objects in real environments [6-9].

There are many studies reported on corrosion or tribo-corrosion behaviour of such thin films or coatings, by considering its practical significance. Recently Wood et al [10] reviewed the tribo-corrosion studies of the coatings and films. The general corrosion/tribo-corrosion behaviour of ZrC_xO_y and TiC_xO_y films in the presence of artificial perspiration solution was studied [4-9] and other work has investigated synergistic effects between corrosion and wear for the purpose of generating tribo-corrosion maps for thermally sprayed coatings [11]. However, there has been no work carried out on the sliding-wear - corrosion behaviour of TiC_xO_y films as a function of electrode potentials and load.

Hence, the objective of the current work was to conduct a tribo-corrosion investigation on a TiC_xO_y film, selected from a previous study [9], Fig.1. The current work is an extension of previous studies, where the most promising film ($TiC_{0.40}O_{1.52}$) as a function of the applied potential and load was identified for corrosion conditions. EIS (Electrochemical impedance spectroscopy) was used to study the specific behaviour of the film before and after the sliding process. Various tribo-corrosion mechanism, wastage and synergism maps, as a function of applied potential and load were also constructed based on the results.

2. Experimental details

2.1. Film preparation

Samples have been prepared by reactive DC magnetron sputtering, from a Ti target (200×100×6 mm^3), with 12 cylindrical C pellets (10 mm diameter each, occupying an average area of (785 mm^2) incrusted in its erosion zone. The substrate was M2 tool steel. The details on this film preparation conditions can be found elsewhere [9]. The Ar flow was kept constant at 60 sccm and the oxygen flow rate was set to 4 sccm (corresponding to a partial pressure of 3.5×10^{-2} Pa). The working pressure was approximately constant at 0.4 Pa and the samples were ground as surface preparation.

The chemical composition of the film was investigated with a Cameca SX-50 Electron Probe Micro Analysis (EPMA), operating at 15 keV as acceleration voltage. Quantification of composition of the elements was performed by comparing the peak intensity in the sample and in standards for each element, and applying a ZAF correction to the results. The structure and phase distribution of the coatings were accessed by X-ray diffraction (XRD), using a conventional Philips PW 1710 diffractometer, operating with Cu $K_{\square}$ radiation, in a Bragg-Brentano configuration. The oxygen fraction in the selected film was determined by the ratio between the s oxygen concentration and the sum of both oxygen and carbon concentrations: $f_O = C_O/(C_O+C_C)$. Ball cratering tests were used to measure the thickness of the film. The hardness, H, was evaluated by depth-sensing indentation, using a Fisherscope H100 equipment at maximum load of 30 mN. Correction of the geometrical defects in the tip of the indenter, thermal drift of the equipment and evaluation of the uncertainty of the initial contact were carried out [12, 13]. Surface and cross-section morphological features of the films were studied by scanning electron microscopy (SEM) and atomic force microscopy (AFM), while surface defects were characterized by optical microscopy. A summary of the film properties is given in Table 1.

2.2. Initial study on corrosion behavior

Corrosion behavior of the selected thin film was studied by conducting open-circuit potential (OCP) during 600 s and potentiodynamic polarization tests, in both substrate (high-speed steel (AISI M2)) and $TiC_{0.40}O_{1.52}$ film, between -0.8 V to +2.0 V at a scan rate of 2 $mV.s^{-1}$. The Potentiostat/galvanostat used was PGP201 (Radiomater analytical, Denmark), controlled by the Voltamaster-1 software.

2.3. Tribo-corrosion

A schematic diagram of the tribocorrosion experimental apparatus is shown in Fig. 2. The reciprocating sliding test apparatus, (Plint TE-67/R) was supplied by Phenoix Tribology Ltd (UK). Tests were conducted with an alumina pin on a plate sample at different loads such as 3, 6 and 9 N, a sliding stroke length of 6 mm with a frequency of 1 Hz and an exposed area of 0.95 cm^2. The alumina pin had a truncated cone geometry (the diameter at contact area is approximately 1 mm). The plate sample was connected as a working electrode in an electrochemical cell. The electrolyte, artificial sweat solution was prepared (composition is given in Table 2) and ammonia (NH_3) was added to attain the pH of 4.49 $\pm$0.01. The solution is a simplified variation of that formalised in the European Standard EN 1811:1998 [14], contained in an acrylic cell with a volume of approximately 20 ml. A saturated calomel electrode (SCE) was used as the reference electrode and a platinum wire was used as a counter electrode.

Experiments were conducted at various applied potentials (-0.9, -0.5, 0 and +0.5 V) and applied load (3-6-9N) as explained in Table 2. Each test consisted on the following steps:

(a) *Cleaning*: The samples were cathodically polarized at -0.9 V vs. SCE during 180 s for the purpose of cleaning.

(b) *Initial stabilization*: A selected potential of -0.5 V was applied during 600 sec.

(c) *EIS before sliding*: Electrochemical impedance spectroscopy (EIS) was performed in the frequency range of 100 kHz to 15.823 mHz, with an ac sine wave amplitude of 10 mV applied to the electrode, keeping the sample under potentiostatic control, i.e., at a selected potential (e.g., -0.5 V).

(d) *Sliding*: The alumina pin was placed in contact with the plate sample. The reciprocating sliding tests were conducted during 900 s, at a selected potential (e.g., -0.5 V).

(e) *Stabilization before and after sliding*: To achieve electrochemical stabilization of the samples before and after the sliding process, the selected potential (e.g., -0.5 V), was applied for a period of 180 sec.

(f) *Final stabilization*: After the stabilization, the pin was removed from contact with the sample, which was left stabilizing, at a selected potential (e.g., -0.5 V), during 600 sec,

(g) *EIS after the sliding*: Another EIS test was conducted after the sliding in order to characterize the behavior of films.

As explained in Fig. 3, the evolution of current and friction coefficient were monitored as a function of time. At the end of the test, the pin and sample were ultrasonically cleaned in propanol and then in distilled water. Each experiment was repeated twice, to estimate the expected error in the tests. For EIS data simulation the ZView software was used. The wear volume was determined by profilometry, using a Perthometer S5P surface measuring and recording instrument, by measuring the cross-sectional area and stroke length. The cross sectional area and depth of the wear profiles were measured with the help of Autocad 2006.

3. Results and Discussion

3.1. Corrosion behavior

Fig. 4 shows the potentiodynamic polarization curves of the $TiC_{0.40}O_{1.52}$ film. For comparison purposes, the result obtained in the substrate is also showed. The results indicate an enhancement in corrosion resistance for the films which confirms the results of the previous study [9]. A small passive plateau between 0.0 V and 0.5 V in the thin film is detected. For the tribo-corrosion study, four values of potential were selected (-0.9, -0.5, 0, +0.5 V), as shown in the Fig. 4. A cathodic potential, 0.9 V, a potential near the E_{corr}, -0.5 V and other potentials corresponding to anodic conditions, 0.0 V and 0.5 V, were chosen.

3.2. Tribo-corrosion behavior at various potentials and loads

3.2.1 Evolution of current as a function electrode potentials and load

Fig. 5 (a-c) shows the evolution of current as a function of time for the various potential values tested during the sliding period at the selected loads, 3N, 6N and 9N respectively. During sliding, the corrosion current shows slight increase with time. Further, it is clear that the value of current at highest potential is very high, compared to that at lower potentials, indicating a higher corrosion rate. Also the sharp increase in corrosion current observed immediately after the start of the sliding process is higher as the applied potential becomes more anodic. Fig. 5(d), shows the variation in current for 5 cycles at high values of potential, +0.5V and at load of 5N . It is interesting to note that the current variation is consistent in each cycle irrespective of the applied potential. The current variation during the rubbing is not very significant. However it is known that the changes in the tribological conditions in the contact, will affect the current evolution [15]. The main factors are, build up of third body (wear debris and corrosion

products) in the contact zone, microstructural changes of the metal or pin, and the material transfer to the counter body.

Significant amounts of wear debris are observed outside the wear track in the wear tests at higher potential values when compared to those at lower potential values. Other studies have reported that the wear debris may undergo dissolution or passivation effects, depending on the potential values, which in turn may affect the values of the current and tribocorrosion behaviour [15]. It is interesting to note the reduction in the friction coefficient values as the potential increases. This is possibly due to the presence of the corrosion products and wear debris in the wear path and their possible interactions [16].

The reciprocating motion of the tribometer, may also influence the evolution of current, which is a periodic function of the pin motion. In the present configuration, the pin moves at constant speed during a forward stroke, and remains stationary for a few milliseconds before changing direction. The above effects during each cycle will be likely to influence the current evolution and tribocorrosion interaction, see, Fig. 5 (d).

3.2.2 Evolution of friction coefficient as a function electrode potentials and load

The evolution of friction coefficient values as a function of time and selected potential and different loads (3 N, 6 N and 9 N) are is shown in Fig 6 (a-c). The figures show that, in all the cases, the friction coefficient attains a steady state value after a short initial period. Further, there is a general tendency to a drop off of the values of the friction coefficient, as the potential increases, except at 6 N. In the case of 3 N and 9 N, the lowest values of friction coefficient were obtained at the highest potentials. Such variation is clearly influenced by the wear debris and corrosion products at the contact zone. Even the mechanisms of the sliding process may change from two to three body, by the presence of the wear debris in the contact zone. However, the visible difference

in the behavior at 6 N, indicates that, the evolution of friction coefficient at different potentials can be influenced by other factors. There are no significant difference in the evolution of friction coefficient at different loads and as in the previous case, did not show a definite pattern in the variation. Further, in the previous study it was shown that friction coefficient values might increase or decrease, associated with the decrease and/or fluctuations in corrosion current, which is exhibiting the complexity of such dynamic tribocorrosion systems [10,16].

3.3. Electrochemical impedance spectroscopy (EIS) analysis

3.3.1. Bode phase plot and Bode Z plot

The results of the EIS tests before and after sliding are presented in Figs. 7 (a-b) and 8 (a-b). Bode phase plot (Frequency vs. Phase angle) and Bode impedance |Z| plot (Frequency vs. impedance modulus |Z|) before sliding at 3 N are shown in Fig. 7 (a) and (b), respectively. As it can be observed, it is clear that before sliding at -0.5 V ($E_{(i=0)}$) and at -0.9 V (potential in the cathodic branch), the film exhibited good corrosion performance as the potential corresponds to the cathodic conditions. On the other hand, at 0.0 V and +0.5 V, at either ends of the potential spectrum tested, a decrease in the corrosion resistance was detected. The impedance of the film had the minimum value at +0.5 V, when compared with the other potentials, probably due to the fact that, at this potential, the pitting corrosion commences (see Fig. 4).

Fig. 8 (a) and (b) show the Bode phase plot and Bode Z plot obtained after sliding at 3 N. It is clear that the good corrosion behavior of the film is kept after sliding at -0.5 and -0.9 V. These results suggest that, at these potentials, the protective characteristics of the film are not removed by the sliding process. On the other hand, at 0.0 and 0.5 V the corrosion resistance of the film suddenly decreases. This decrease is more pronounced at 0.0 V (see Fig. 8 (b)) probably due to the disappearance of the initially formed

passive film after the sliding process. In case of +0.5 V (pitting potential), the decrease in the corrosion resistance after the sliding test is less apparent than at 0.0 V, due to the fact that the surface of the thin film is already degraded by the previous presence of the pitting. The presence of pits will definitely accelerate the film removal and further complete destruction.

Further, Fig. 9 (a-d) show the influence of the load at a selected potential of 0.0 V, before and after the sliding process. Figs. 9 (a) and 9 (b) show the Bode Z plot before and after sliding process, respectively, while Figs. 9 (c) and 9 (d) show the Bode phase plots before and after sling, respectively. As expected, before sliding at all the loads, 3, 6 and 9 N, the impedance of the system (see Fig. 9 (a)) is higher than that showed after sliding (see Fig. 9 (b)). It is important to note that before sliding at 3 and 9 N, the film showed similar impedance values, which are slightly higher than that observed at 6 N (see Fig. 9 (a)). Possibly this is related to the experimental set-up/conditions and surface conditions of the sample. Nevertheless after sliding, at all loads, the film had very similar impedance values. Bode phase plots show also a pronounced decrease in the phase angle (from -35º (6 N) and -45º (3 N and 9 N) to -10º (3, 6 and 9 N)) after sliding process (see Fig. 9 (c) and 9 (d)), indicating the strong degradation of the film at this potential (0.0 V) at all loads. These results suggest that at that potential, when the formation of a passive layer is yet incipient, the degradation process during the sliding is independent of the load.

3.3.2 EIS model

Results of the EIS experiment were modeled by an electrochemical equivalent circuit, which describes the corrosion behavior of each sample. In the present work, a simple equivalent circuit composed by the electrolyte or solution resistance (R_s) in series with a constant phase element (CPE) in parallel with the polarization resistance

(R_p), was proposed. The impedance of a CPE is defined by $Z_{CPE} = 1/((jw)^n C)$, where $j = \sqrt{(-1)}$ and $w = 2\pi f$, and the exponent 'n' of the CPE is related to non-equilibrium current distribution due to surface roughness [17-18]. The parameter 'C' is a constant, representing true capacitance of the oxide barrier layer. The variation of polarization resistance (R_p) and film capacitance (C_f), as a function of load and potential are shown in Fig. 10 and 11. Further all the values with their expected error are listed in the Table 3.

The parameter R_s, represents the average solution resistance is 125 $\Omega.cm^2$ (the range is (110-140 $\Omega.cm^2$), irrespective of before or after the sliding. The Polarization resistance, R_p, at the applied potential values of -0.9 and -0.5 V, shows high values as it corresponds to cathodic conditions. It is interesting to note that R_p values after the sliding are approximately half of the same before sliding, which shows the removal of film and subsequent effect created after the sliding. Further, R_p values are significantly low for 0.0 V and even lower for +0.5 V, showing the heavy damage occurred at the film surface, at high anodic potential. As already indicated above samples polarized at +0.5 V (pitting potential) showed the lowest R_p values, both before and after sliding process, when compared with the other samples probably due to the presence of the pits.

The C values are almost constant at the applied potential values of -0.9 and + 0.5 V, before and after the sliding (Fig. 11). However, at high potentials, interestingly C exhibit high values after the sliding, which may be due to the accumulation of wear debris and corrosion products, resulting from the complete destruction of the film [9]. The values of n, almost constant in all the conditions, were found to be in the range of 0.6-0.7, indicating that the corrosion interface deviated from a perfect ideal capacitor [16]. Theoretical model predictions are in good agreement with the experimental data (percentage of error is below 6 %, see the Table 3). From the EIS analysis it is clear

that, as the potential increases, the passive oxide layer on the film becomes more porous and resistance to charge transfer decreases at the corrosion interface [18-20]. It is also clear that the best and worst corrosion behavior correspond to samples polarized at pitting potential -0.5 V and +0.5 V.

Also, it is interesting that at -0.9 and -0.5 V, before and after sliding, the worst corrosion behavior occurs at loads of 6 N. However at 0.0 V and +0.5 V (potentials in the passive plateau), the degradation processes during sliding is independent of the load. The structure of the film has also a strong influence on the EIS results, as explained in detail in previous work [9].

3.4. Variation of wear volume as a function of load and selected potential

Wear-corrosion volume loss was estimated from the wear track, obtained during the tribocorrosion test, as explained in the experimental procedures. The following terms were used to explain the total wear-corrosion volume loss and their interactions. The methodology was developed by Yue and Shi [20], in the wear-corrosion analysis. If:

$$K_{wc} = K_w + K_c \quad (1)$$

where K_{wc} is the total wear-corrosion, K_w is the total wear loss due to sliding wear and K_c is due to corrosion, than the volume loss due to the corrosion, K_c, is derived using Faraday's law, e.g.:

$$K_c = Q/ZF \quad (2)$$

$$K_c = MIt/ZF \quad (3)$$

where ‘Q’ is the charge passed, ‘F’ is Faraday’s constant (96500 $C.mol^{-1}$), ‘Z’ is the number of electrons involved in the corrosion process (in the current study, it is assumed to be 2), ‘I’ is the total current, ‘t’ the exposure time and ‘M’ is the atomic mass of the material. The M is calculated by considering the atomic percentage of components of the film. More details on the calculation of different terms are explained Appendix A.

The results of the various contributions to wear volume loss are given in Table 4 and Fig. 12(a-d). Fig 12 (a) shows the variation of total wear-corrosion wear volume (K_{wc}) as a function of applied load, at the selected potentials -0.9, -0.5, 0.0 and +0.5 V, respectively. As expected, there is an increment in the K_{wc} as the load increases. The good behaviour at -0.5 V may be due to the formation of passive films (same trend was observed with EIS analysis, Section 3.3 and 3.4). Further, there is a significant increment in the total volume loss when it changes from -0.5 to +0.5, as it is shown in the Fig. 12(a). It is interesting to notice the good agreement between the variations of wear-volume as a function load with the Archard equation, which indicates a direct increase of wear rate with load [23].

Further, Figs 12 (b), (c) and (d) show the variation of K_{wc}, K_w, and K_c as function of applied load, at the selected potential -0.5, 0.0 and +0.5 V respectively. As expected, there is an increment in both K_{wc} and K_w, as load increases. However K_c shows only small variation. Interestingly, there is a reduction in the K_c value at higher loads, possibly due to the high contact pressure at the contact zone, and the possible interactions with solution, wear particles and films surface.

The superior behaviour at -0.5 V may be due to the formation of a passive film (a similar same trend was observed with EIS analysis), Fig. 12 (b). It is clear that K_{wc} and K_w did not show significant differences which demonstrates the predominant driving

mechanism in the present study is wear. Also the severity of the contact may increase due to the pin-on-plate contact configurations, which accelerates the wear mechanisms [9].

As observed from Potentiodynamic curves, Fig. 5, the corrosion behaviour is significantly affected by increases in potential, Fig. 12. The corresponding pitting behaviour, passivation or repassivation, etc, may also have a role in driving the degradation involved in the process [9, 24, 25]. In the previous study, it was observed that the structure of the films has a strong influence on their tribocorrosion behaviour, even more than their hardness and thickness [9]. The structure of the film is tailored by the processing parameters, surface conditions and many other parameters; it is a very difficult task to have one which is ideal for tribocorrosion resistance. The tribological studies on tungsten carbide coating, reported that fine closely packed structures exhibit good performance due to their superior elastic behaviour and hardness [9, 26-27].

3.5 Construction of maps as a function of load and potential

Wear maps are the schematic diagrams of tribological processes as a function of several parameters considered in the test [22-23]. To understand the processes and mechanisms related to tribology and tribocorrosion, simple two-dimensional or three dimensional graphs may not be sufficient because of the complexity, and enormous number of factors involved in the processes. Hence, using the mapping approach, it is very useful to have clear pictures of the observed behavior of the tested film. In the case of tribocorrosion i.e., erosion-corrosion, sliding wear-corrosion, microabrasion-corrosion, Stack et al. has demonstrated the application of such mapping methodologies to such tribocorrosion system [24-25, 28-30].

There are some terms are included in studying the tribocorrosion interactions and the synergistic effects. The total wear volume loss in the Equation 1, $K_{wc}= K_w + K_{c,}$ can be split into two groups, $K_{wc} = (K_{wo} + \Delta K_w)$ {wear part) $+ (K_{co} + \Delta K_c)$ {corrosion part}

K_{wo} = Wear volume loss in the absence of corrosion, ΔK_w = Change in the wear rate loss due to corrosion, K_{co} = Volume loss due to corrosion in the absence of wear. ΔK_c = Change in the corrosion rate due to wear.

Further explanation on the calculation of each terms are included in the Appendix A.

Therefore, an attempt has also been made to construct different maps in the current study. The developed mechanisms map, wastage map and synergism map are explained below.

3.5.1 Mechanisms map

In order to understand the synergistic effects, K_c/K_w ratio was estimated, as shown in Table 4. As it is observed from the literature, Stack et al. [24-25], in their extensive studies on erosion-corrosion and wear-corrosion, have established various regimes to identify the dominating mechanisms in the tribocorrosion process. The major criteria are listed below.

$$K_c/K_w \leq 0.1 \quad \text{(wear)} \quad (4)$$

$$0.1 < K_c/K_w \leq 1 \quad \text{(wear- corrosion)} \quad (5)$$

$$1 < K_c/K_w \leq 10 \quad \text{(corrosion- wear)} \quad (6)$$

$$K_c/K_w > 10 \quad \text{(corrosion)} \quad (7)$$

Based on the above criteria and polarization curves, the mechanism map has been developed as shown in Fig. 13. Low potential and load correspond to the wear dominated region. However, as the potential increases, a wear dissolution region is

observed. Before attaining wear passivation behaviour there is a transition region, termed the wear active-passive transition. Finally, at high potential, the wear dissolution region appears again. It is interesting to observe the changes and interplay of the mechanisms as a function of load and applied potentials.

Further, the transition of the mechanisms can be shown by the schematic diagram of Fig. 16, based on the observations during the tribocorrosion tests and surface characterisation of the worn surface. In the cathodic region, -0.9 V, the wear scar observed was very clear with a well defined boundary. However, as the applied potentials increased to the anodic region (-0.5 and 0 V), the change of the wear scar is very vivid, i.e., initially the boundaries are irregular and lead to the next stage, where the Delamination of the film observed. At the high potential value, +0.5 V, it is interesting to see that the film, in the exposed area, is removed, which leads to significant wear-corrosion loss. Such transition mechanisms were very clear in SEM images, as shown in Fig. 15 (a-e). Fig. 15 (a) shows the pit formed on the worn surface at electrode potential of +0.5 V, while Fig. 15 (b) shows the clear wear path formed on the surface after the tribocorrosion tests.

The delamination of the film is shown in Fig. 15 (c), which is due to the combined action of wear and corrosion, while Fig. 15 (d) shows the effect of dissolution of the substrate material, leading to a complete film removal during the tribocorrosion process. Finally Fig. 15(f) shows the enlarged view of a region of the wear path in Fig. 15 (e).

3.5.2 Wastage map

The wastage map has been constructed as a function of applied potential and load, as shown in Fig. 16. The criteria has been selected as:

$$K_{wc} \leq 0.05 \quad \text{(low)} \tag{8}$$

$$0.05 < K_{wc} < 0.25 \quad \text{(medium)} \tag{9}$$

$$K_{wc} \geq 0.25 \quad \text{(high)} \tag{10}$$

The low wastage region is exhibited by the low potential, below -0.25 V (the value approximated through linear interpolation) and low load, as expected. The expansion of the medium wastage zone as a function of load is an indicative of the influence of the load on the total volume. Similar behavior can be observed in the case with high wastage zone, which is located at high anodic potential [28-29].

3.5.3 Synergism map

Wear-corrosion synergism map also can be constructed as a function of applied load and potential, as shown in Fig. 17, to demonstrate the synergistic effect as defined in the Table 4. By considering the various terms involved, the boundary conditions can be specified as follows:

$$\Delta K_w / K_{wo} \leq 1 \quad \text{(low synergism)} \tag{11}$$

$$1 < \Delta K_w / K_{wo} \leq 10 \quad \text{(medium synergism)} \tag{12}$$

$$\Delta K_w / K_{wo} > 10 \quad \text{(high synergism)} \tag{13}$$

There are studies also conducted on the beneficial effect of the corrosion, known as negative synergism. However, in the current study the predominant effect is due to the corrosion to accelerate the wear [9, 11].

3.6 Limitation and scope

The current study was focussed only on one film to understand its tribocorrosion behaviour. The variation of wear-corrosion volume was studied as a function of two parameters: i) the corrosion parameter, i.e., applied potential and; ii) the mechanical parameter, i.e., load. This study clearly showed that there is a need of such studies to consider other parameters, even selecting intermediate values of the same parameters. Although the maps give some pictures on the tribo-corrosion behaviour, as shown for other studies in the area [31-36] it is based on the experimental data, and not at this stage, a mathematical model of the process [37]. Hence, in future there is significant scope to extend the methodology employed in the current study, and employ modelling techniques to verify the data, in order to establish these boundaries theoretically.

4. Conclusions

A detailed study on the tribocorrosion behavior of a TiC_xO_y film ($TiC_{0.40}O_{1.52}$) was conducted as a function of electrode potential and applied load. The main conclusion can be summarized as follows: The enhancement of corrosion due to wear was very clear at the high potential.

- EIS analysis was consistent with the above observation.
- Tribo-corrosion mechanisms and wastage maps have been developed as a function of applied and electrode potential.
- A synergism map has also been constructed to display the effect of load and electrode potential on the degradation rate.

Acknowledgements

The authors would like to thank the financial support from FCT (Foundation of Science and Technology), Portugal, through individual projects.

References

1. Eerden M. Products Finishing 2003;54-59.

2. Rocha LA, Ariza E, Ferreira J, Vaz F, Ribeiro E, Rebouta L, Alves E, Ramos AR, et al. Surface and Coatings Technology 2004;180-181:158-163.

3. Foneca C, Vaz F, Barbosa MA. Corrosion Science 2004;46:3005-3018

4. Gu JD, Chen PL. Surface and Coatings Technology 2006;200:3341-3346.

5. Vaz F, Cerqueira P, Rebouta L, Nascimento SMC, Alves E, et al. Surface and Coatings Technology 2003;174-175:197-2003.

6. Fernades AC, Vaz F, Ariza E, Rocha LA, Ribeiro ARL, Viera AC, Riviere JP et al. Surface and coatings Technology 2006;200:6218-6224.

7. Ferreira SC, Ariza E, Rocha LA, Gomes JR, Carvalho P, Vaz F, Fernandes AC, L. Rebouta, et al. Surface and Coatings Technology 2006;200:6634-6639.

8. Ariza E, Rocha LA, Vaz F, Cunha L, Ferreira SC, Carvalho P, Rebouta L et al. Thin Solid Films 2004;469-470:274-281.

9. Mathew MT, Ariza E, Rocha LA, Fernandes AC,Vaz F. Tribology International 2008;41:603–615.

10. Wood. RJK. J. Phys.D:Appl. Phys. 2007;40:5502-5521.

11. Stack MM, Abd El Badia TM. Wear 2006;261:1181-1190

12. Antunes JM, Cavaleiro A, Menezes LF, Simões MI, Fernandes JV. Surface and Coatings Technology 2002;149:27

13. Parreira NMG, Carvalho NJM, Vaz F, CavaleiroA. Surface and Coatings Technology. 2006;200:6511.

14. European Standard EN 1811:1998. Reference test method for release of nickel from products intended to come into direct and prolonged contact with the skin.

15. Jemmely P, Mischler S, Landolt D, Tribology International 1999;32:295-303.

16. Pontiaux P, Wenger F, Drees D, Celis JP. Wear 2004;256:459-468
17. Ariza E, Rocha LA, Materials Science Forum 2005;492-493:189-194.

18. Robert WH, Yang CC, Huang CA, Chen YS, Materials Science and Engineering A 2004;380:100-109.

19. Aziz-Kerrzo M, Conroy KG, Fenelon AM, Farrell ST, Breslin CB. Biomaterials 2001;22:1531-1539.

20. Shukla AK, Balasubramanian R, Bhargava S. Intermetallics 2005;13:631-637.

21. Fernandes AC, Carvalho P, Vaz F, Lanceros-Méndez S, Machado AV, Parreira NMG et al., Thin Solid Films 2006;515:866.

22. Yue Z, Zhou P, Shi J., Proc. Conf. Wear of Materials, ASME (Luedema K.C. Ed), New York 1987; 763-768.

23. Archard JF. J. Appl. Phys. 1953;24:981

24. Stack MM, Mathew MT, Jawan H. Tribology International 2005;38 9:848-856.

25. Stack MM. Tribology International 2002;35:681-689.

26. Zhang H, Li DY. Wear 2003;255:924-32

27. Wu P-Q, Celis JP. Wear 2004; 256:480-90.

28. Stack MM, Pungwiwat N. Wear 2004:256 5:565-576

29. Stack MM, Chi K. Wear 2003: 255:456-465

30. Stack MM, Abd El Badia TM. Wear 2008:264:826-837.;

31. Mathew MT, Matijevic B, Stack MM, Rocha LA, Ariza E, Tribology International 2008: 41:141-149.

32. Muñoz AI, Julián LC, Electrochimica Acta, In Press, Accepted Manuscript, Available online 4 May 2010

33. Azzi M, Paquette M, Szpunar JA, Klemberg-Sapieha JE, Martinu L, Wear 2009; 267, 5-8, 860-866

34. Purandare YP, Ehiasarian AP, Stack MM and Hovsepian P Eh, Surface and Coatings Technology 2010: 204, 8, 1158-1162,2010.

35. Stack MM and Abdelrahman GH, Tribology International 2010: 43, 7, 1268-1277

36. Stack MM, Rodling J, Mathew MT, Jawan H, Huang W, Park G and Hodge C, Wear (in press, published on-line 1 May 2010) doi:10.1016/j.wear.2010.04.022

37. Stack MM, Abdelrahman S,M and Jana BD, Wear, 268, 3-4, 533-542, 2010.

Appendix A: Calculations of terms used tribocorrosion interaction analysis, K_{wc}, K_w, K_c

As mentioned in the manuscript, (Equation 1) The total wear volume loss due to wear and corrosion, $K_{wc} = K_w + K_c$ (A.1)

Where,

K_{wc} = The total wear-corrosion, K_w = The total wear loss due to sliding wear

K_c = Wear volume loss due to corrosion,

Further, $K_{wc} = K_w + K_c$, can be divided in to two groups

$$= (K_{wo} + \Delta K_w) + (K_{co} + \Delta K_c) \quad (A.2)$$

K_{wo} = Wear volume loss in the absence of corrosion,, ΔK_w = Enhancement in the wear volume loss due to corrosion,K_{co} = Volume loss due to corrosion in the absence of wear. ΔK_c = Enhancement of corrosion due to wear

More explanation on the calculation of each term is given below

1. Total wear volume loss, (K_{wc})
The total wear volume, K_{wc}, estimated from the wear scar dimensions.

2. Calculation of mass loss by corrosion (K_c)
The volume loss due to the corrosion, K_c, is estimated using Faraday's law, (as mentioned Equation 2 and 3)

$$K_c = Q/ZF \quad (A.3)$$

$$K_c = MIt/ZF \quad (A.4)$$

where 'Q' is the charge passed, 'F' is Faraday's constant (96500 $C.mol^{-1}$),

Z' is the number of electrons involved in the corrosion process (in the current study, it is assumed to be 2), 'I' is the total current, 't' the exposure time, 'M' is the atomic mass of the material or equivalent weight.

3. K_{wo} = Wear volume loss in the absence of corrosion

Wear volume loss in the absence of corrosion is estimated from total wear volume loss at cathodic potential (-0.9V). It is assumed that, there is no corrosion at this potential. So K_{wo} = K_{wc} at -0.9 V)

4. ΔK_w = Enhancement in the wear volume loss due to corrosion

By referring to equation A.1 and A.2 $K_{wc} = K_w + K_c$

$$= (K_{wo} + \Delta K_w) + (K_c) \quad \text{(A.5)}$$

Hence the enhancement in the wear volume loss due to corrosion is

$$\Delta K_w = K_{wc} - (K_{wo} + K_c) \quad \text{(A.6)}$$

5. K_{co} = Volume loss due to corrosion in the absence of wear

Volume loss due to pure corrosion is calculated from the evolution of current at corresponding potential and using faradays law, during the electrochemical tests, without wear.

6. ΔK_c = Enhancement of corrosion due to wear

Enhancement of corrosion due to wear is estimated from the equation, (A.2),

$$K_{c,} = K_{c,o} + \Delta K_c$$

Hence, $$\Delta K_c = K_c - K_{c,o} \quad \text{(A.7)}$$

Table Captions

1. Experimental details
2. Details of tested film
3. Values of the parameters obtained during the EIS analysis
4. Wear-corrosion volume data (K_{wc}, K_w, K_c)

Figure Captions

1. General tribocorrosion behaviour of the TiC_xO_y films: the outcome of the initial study, showing two of the most promising films for tribocorrosion resistance.
2. Schematic diagram of reciprocating pin/plate tribometer and electrochemical cell used in the test.
3. Tribocorrosion process, evolution of current and friction coefficient as a function of sliding durations
4. Potentiodynamic curves for the TiC_xO_y film and substrate materials, showing the selected potential.

5. (a-d) Evolution of current as a function of selected potentials (-0.9V, -0.5V, 0V, +0.5V) at different load (a) 3N (b) 6N (c) 9N, (d) Variation of current for 5 cycles at +0.5V, 9N
6. (a-c) Evolution of friction coefficients as a function of selected potentials (-0.9V, -0.5V, 0V, +0.5 V) at different loads at (a) 3N (b) 6N (c) 9 N
7. (a-b) Bode phase plot (Frequency vs. Phase angle) and Bode Impedance (IZI) plot (Frequency vs. Impedance modulus |Z|) before sliding at selected potentials
   (a) Bode phase plot, 3N, (b) Bode Impedance (IZI) plot, 3N
8. (a-b) Bode phase plot (Frequency vs. Phase angle) and Bode Impedance (IZI) plot (Frequency vs. Impedance modulus |Z|) at selected potentials after sliding.
   (a) Bode phase plot, 3N, (b) Bode Impedance (IZI) plot, 3N
9. (a-d) Bode phase plot (Frequency vs. Phase angle) and Bode Impedance (IZI) plot (Frequency vs. Impedance modulus IZI) at different load (3, 6 and 9 N) before and after the sliding.
   (a) Bode phase plot, before sliding, 0.0 V.
   (b) Bode phase plot, after sliding, 0.0 V
   (c) Bode Impedance (IZI) plot, before sliding, 0.0 V
   (d) Bode Impedance (IZI) plot, after sliding, 0.0 V
10. Variation of Polarization resistance (R_p) as a function of load and potential.
11. Variation of film capacitance (C_f) as a function of load and potential
12. (a-d) Variation of wear-corrosion volume loss (K_{wc}) and corrosion volume loss (K_c) as a function of load (N) (a) Variation of K_{wc}, K_w and K_c , -0.5 V (b) Variation of K_{wc}, K_w and K_c , 0 V (c) Variation of K_{wc}, K_w and K_c , +0.5 V (d) Variation of (K_{wc}):All the results in one scale.
13. Tribocorrosion mechanisms map as a function of applied potential and load

14. A schematic diagram of the possible wear scar profile changes following the tribocorrosion test, showing the effect of increasing applied potential.

15. (a-f) SEM images

    (a) Pits, +0.5 V, 3N

    (b) Cracks, +0.5 V, 3N.

    (c) Dissolution of the substrate, +0.5 V, 3N

    (d) Film completely removed, 0 V, 6N

    (e) Clear wear path.

    (f) Enlarged view of the worn surface

16. Tribocorrosion wastage map as a function of applied potential and load

17. Synergism map as a function of applied potential and load.

18.
19.
20. Tables:
21.
22.
23.
24.

Table 1 Details of the TiC_xO_y film considered in the tests

Sample	Oxygen fraction (f_O)	Thickness (μm)	Ti (at. %)	C (at.%)	O (at.%)	Hardness (GPa)	Number of defects/mm^2
$TiC_{0.40}O_{1.52}$	0.79	4.4±0.1	34.3	13.8	51.9	17.0	197

25.
26.
27.
28.
29.
30.
31.
32.
33.

34.

Table 2 Experimental details

Sample material	TiC_xO_y ($TiC_{0.40}O_{1.52}$)
Pin material	Alumina
Tribometer	Reciprocating sliding tester, pin-on-plate, (Plint TE 67/E)

Frequency	I Hz
Load	3, 6, 9 N
Sliding duration	900 s
Applied potential	-0.9 V (cathodic condition), -0.5 V, 0 V, +0.5 V
Electrodes	SCE –reference electrode, platinum- counter electrode
Solution	**Artificial sweat solution**: composition is NaCl- 7.5 $g.L^{-1}$ KCl-1 $g.L^{-1}$ CH_4N_2O (urea)- 1 $g.L^{-1}$ $C_3H_6O_3$ (lactic acid)- 1 $ml.L^{-1}$ (NH_3 added to adjust the pH of 4.49)

35.
36.
37.
38.
39.
40.
41.
42.
43.
44.

45.

Table 3: The ac impedance parameter values at selected potential and load

ti	Load (N)	Rs ($\Omega.cm^2$)		Rp ($\Omega.cm^2$)		Cf ($F.cm^{-2}$)		n	
		Before sliding	After sliding	Before sliding	After sliding	Before sliding	After sliding	Before sliding	After slidi
	3	124.8(0.17)	124.9(0.29)	9174(3.01)	5044(3.79)	1.5842 E-3 (0.28)	1.6259 E-3(0.55)	0.6303 (0.45)	0.6317(0.4
	6	135.7(0.17)	135.4(0.23)	4071(2.26)	2294(2.05)	2.2197 E-3(0.32)	2.2882 E-3(0.50)	0.5997(0.31)	0.6155(0.4
	9	125.9(0.15)	125.3(0.24)	7332(4.88)	3820(4.44)	2.8109 E-3(0.28)	2.8149 E-3(0.48)	0.6283(0.29)	0.6367(0.4
	3	124.3(0.30)	124(0.28)	10743(3.53)	9783(2.85)	9.6366 E-4(0.30)	9.9923 E-4(0.45)	0.7721(0.33)	0.7738(0.3
	6	136.0(0.37)	139.6(0.35)	7892(2.37)	7067(2.90)	7.7924 E-4(0.62)	8.4777 E-4(0.62)	0.7642(0.40)	0.7694(0.4
	9	131.8(0.37)	129.7(0.45)	11984(3.15)	10035(3.66)	5.5675 E-4(0.65)	1.2971 E-3(0.22)	0.6986(0.36)	0.7182(0.4
	3	132.3(0.48)	127.2(0.26)	1577(1.54)	103.1(3.40)	7.9428 E-4(1.28)	2.9656 E-3(4.90)	0.7444(0.72)	0.5934(2.1
	6	126.1(0.50)	124.2(0.25)	1545(1.56)	92.46(1.09)	7.7538 E-4(1.27)	2.2252 E-3(3.34)	0.7561(0.68)	0.6603(1.3
	9	127(0.55)	124.4(0.24)	613(1.48)	85.29(1.13)	9.551 E-4(2.05)	2.467 E-3(3.43)	0.7583(1.01)	0.6799(1.3
	3	133.3(0.35)	142.8(3.44)	172(2.94)	33.34(3.4)	1.179 E-3(5.01)	4.1207 E-3(4.9)	0.6088(2.03)	0.4665(5.0
	6	111.6(4.32)	113.1(0.90)	168.1(4.4)	36.6(4.1)	1.8563 E-3 (4.5)	4.8957 E-3(3.0)	0.6532(4.6)	0.3456(4.6
	9	126.6(0.46)	113.8(0.69)	160.1(4.7)	37.33(3.48)	2.2118 E-4(6.0)	4.8246 E-3(4.91)	0.7402(2.84)	0.3271(6.4

Values in bracket are the % error in various parameters while fitting the experimental data into the proposed model

46.

47.

48.

49.

Table 4: Wear-corrosion volume loss data at various potentials (a) –0.5 V (b) 0 V (c) 0 +0.5 V.

50.

51.

5 V

K_{wc} (mm^3)	K_c (mm^3)	K_w (mm^3)	K_{wo} (mm^3) (volume loss at –0.9 V)	ΔK_w (mm^3)	K_{co} (mm^3)	ΔK_c (mm^3)	K_c/K_w	$\Delta K_w / K_{wo}$	Δ Δ
3.0388 E-02	2.7402 E-05	3.0361 E-02	2.5989 E-02	4.3720 E-03	1.4390 E-7	2.7258 E-5	9.0253 E-04	0.1658	81
4.3079 E-02	3.1957 E-05	4.3047 E-02	3.1225 E-02	1.1822 E-02	1.4390 E-7	3.1813 E-5	7.4237 E-04	0.3746	18
5.3644 E-02	2.3779 E-05	5.3620 E-02	3.9351 E-02	1.4269 E-02	1.4390 E-7	2.3635 E-5	4.4347 E-04	0.3602	30

52.

V

K_{wc} (mm^3)	K_c (mm^3)	K_w (mm^3)	K_{wo} (mm^3) (volume loss at –0.9 V)	ΔK_w (mm^3)	K_{co}	ΔK_c	K_c/K_w	$\Delta K_w / K_{wo}$	Δ Δ
7.1629 E-02	3.0624 E-04	7.1323 E-02	2.5989 E-02	4.5334 E-02	2.3788 E-5	2.8245 E-4	4.2937 E-03	1.7482	82
7.4553 E-02	3.5035 E-04	7.4203 E-02	3.1225 E-02	4.2978 E-02	2.3788 E-5	6.3681 E-4	4.7215 E-03	1.3807	67

9.7431 E-02	3.1434 E-04	9.7117 E-02	3.9351 E-02	5.8080 E-02	2.3788 E-5	5.6658 E-4	3.2367 E-03	1.4715	10

53.

5 V

K_{wc} (mm^3)	K_c (mm^3)	K_w (mm^3)	K_{wo} (mm^3) (volume loss at –0.9 V)	ΔK_w (mm^3)	K_{co}	ΔK_c	K_c/K_w	ΔK_w / K_{wo}	Δ Δ
2.9331 E-01	1.7709 E-03	2.9154 E-01	2.5989 E-02	2.6555 E-01	2.2026 E-5	3.4104 E-3	6.0743 E-03	10.1856	77
3.4390 E-01	2.0855 E-03	3.4181 E-01	3.1225 E-02	3.1059 E-01	2.2026 E-5	4.0239 E-3	6.1013 E-03	9.9152	77
3.6888 E-01	1.8471 E-03	3.6703 E-01	3.9351 E-02	3.2769 E-01	2.2026 E-5	3.5590 E-3	5.0326 E-03	8.3105	92

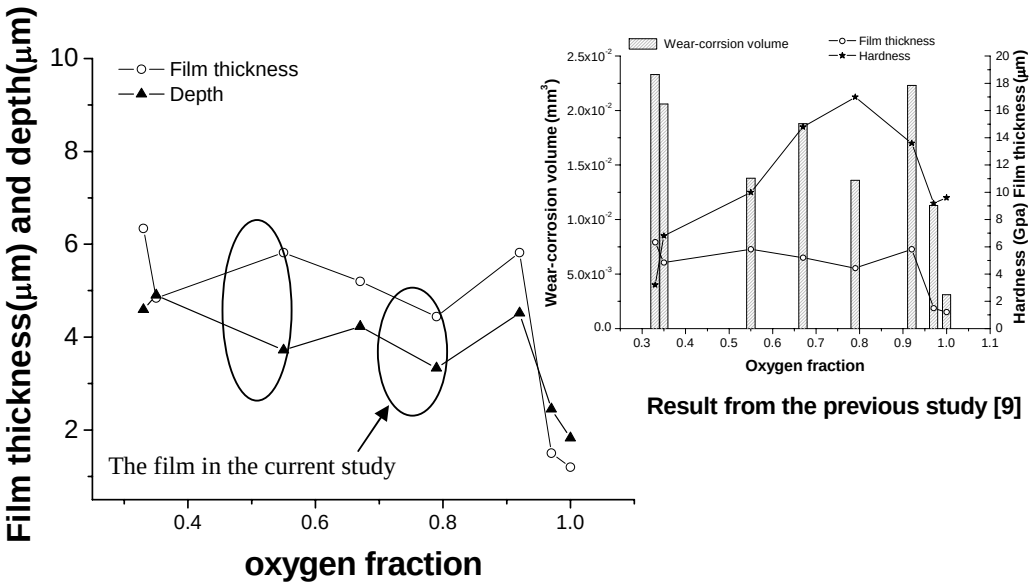

Figure 1 General tribocorrosion behavior of the TiCxOy films: the outcome of the initial study, showing the two of the most promising films for tribocorrosion resistance [9].

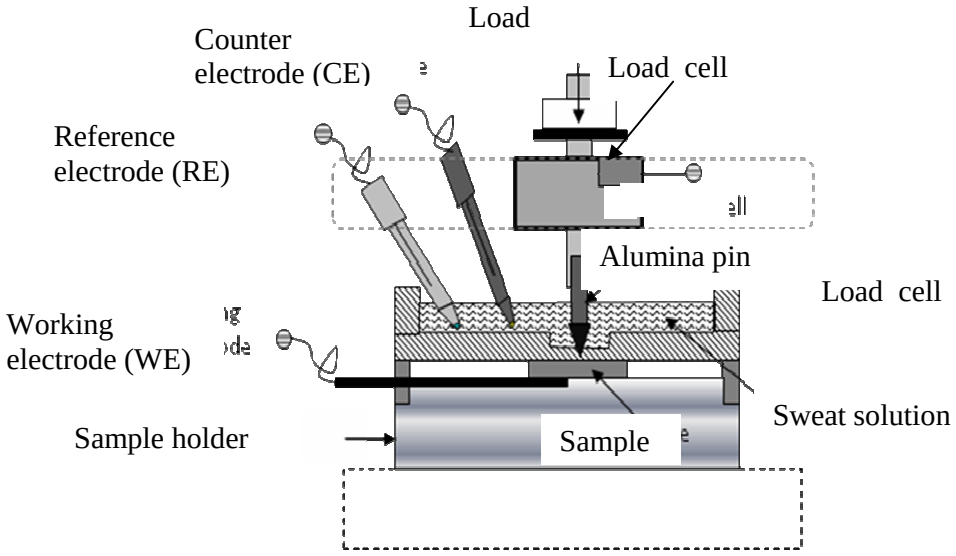

Figure 2 Schematic diagram of reciprocating pin/plate tribometer and electrochemical cell used in the test

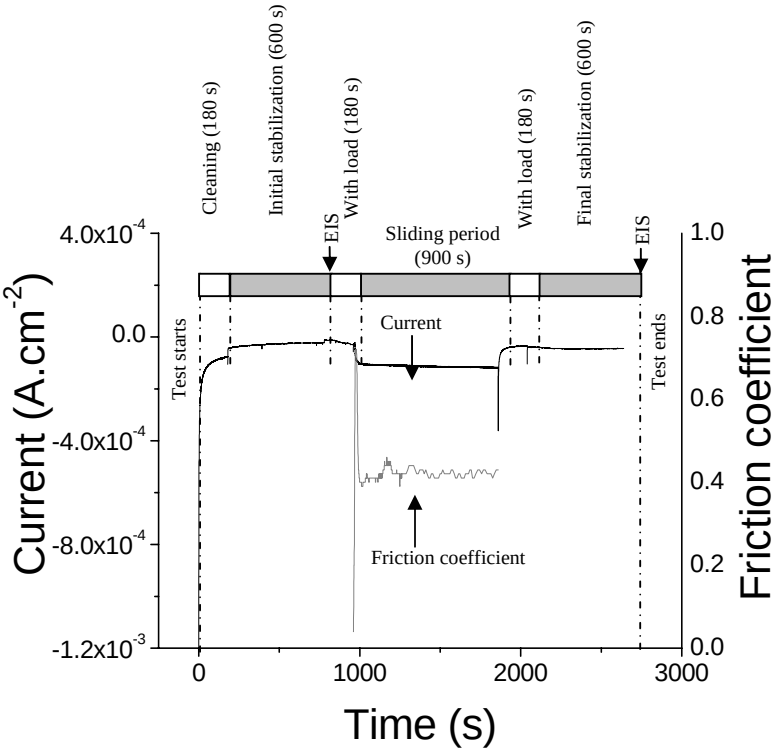

Figure 3 Tribocorrosion process: evolution of current and friction coefficient as a function of sliding duration

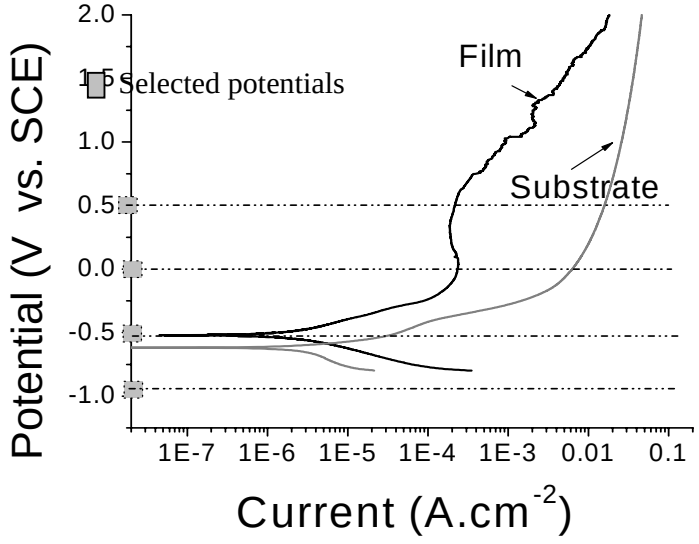

Figure 4 Potentiodynamic polarization curves for the TiC_xO_y film and substrate materials, showing the selected potentials.

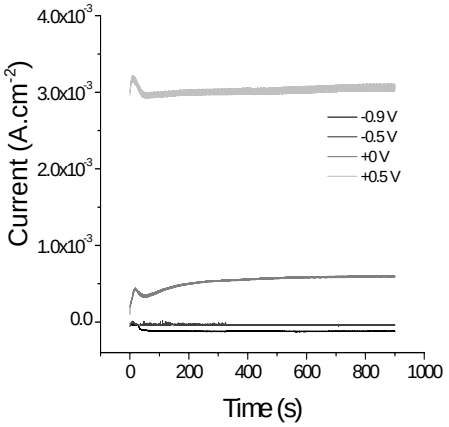

(a) 3N

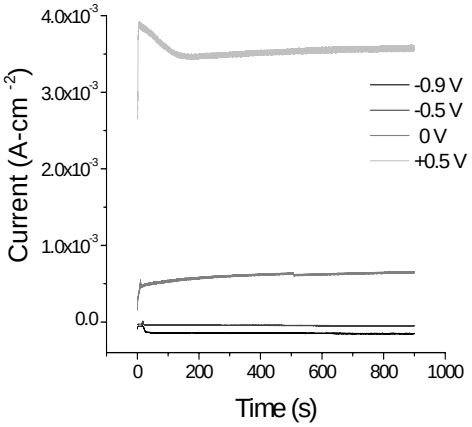

(b) 6N

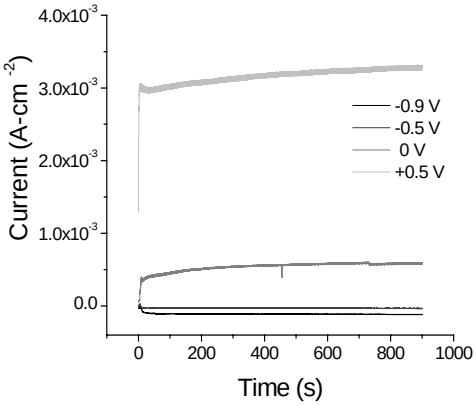

(c) 9N

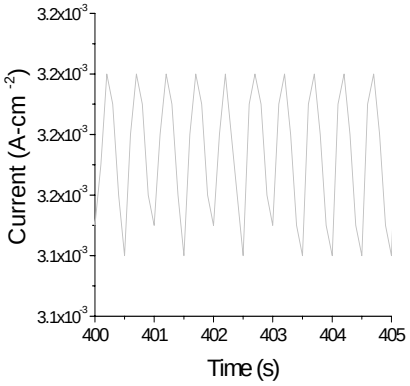

(d) Variation of current for 5 cycles at +0.5V, 9N

Figure 5 Evolution of current as a function of selected potentials (-0.9V, -0.5V, 0V, +0.5 V) at different loads of (a) 3N (b) 6N (c) 9N (d) Variation of current for 5 cycles at +0.5V, 9N

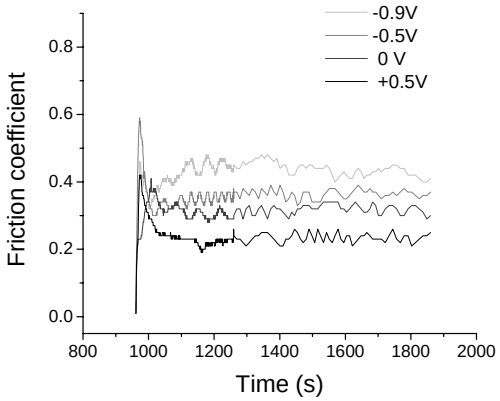

(a) 3N

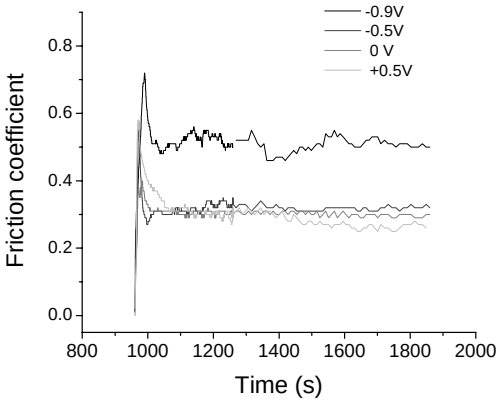

(b) 6N

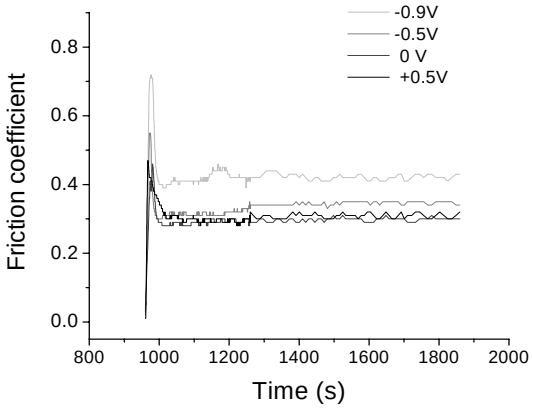

(c) 9N

Figure 6 Evolution friction coefficients as a function of selected potentials (-0.9 V, -0.5 V, 0.0 V, +0.5 V) at different load at (a) 3N (b) 6N (c) 9N

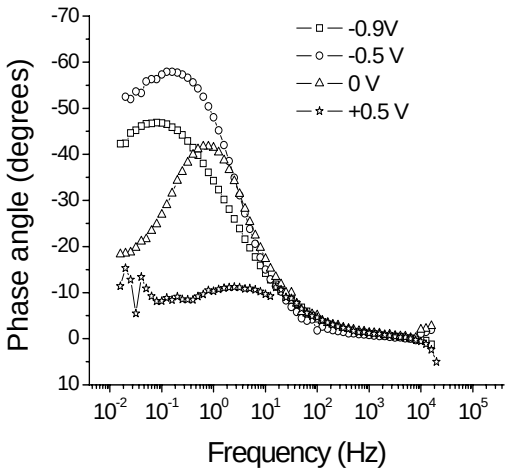

(a) Bode phase plot, 3N

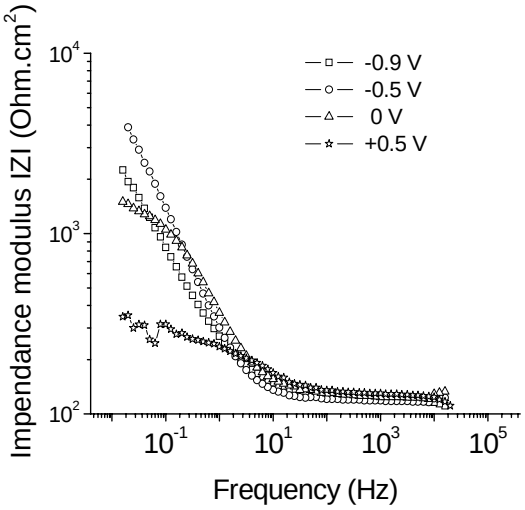

(b) Bode impedance (|Z|) plot, 3N

Figure 7 (a-b) Bode phase plot (Frequency vs. Phase angle)) and Bode Z plot (Frequency vs. Impedance modulus |Z|) before the sliding at selected potentials and load of 3N

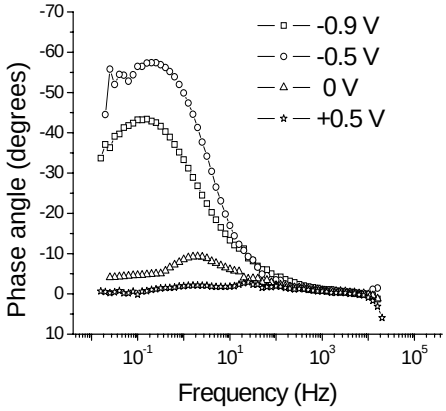

(c) Bode phase plot, 3N

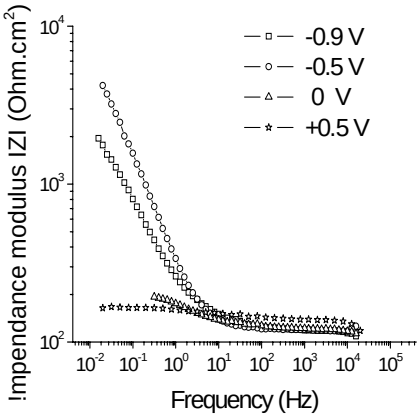

(d) Bode impedance (Z) plot, 3N

Figure 8 (a-b) Bode phase plot (Frequency vs. Phase angle) and Bode Z plot (Frequency vs. Impedance modulus |Z|) after the sliding at selected potentials and load of 3N

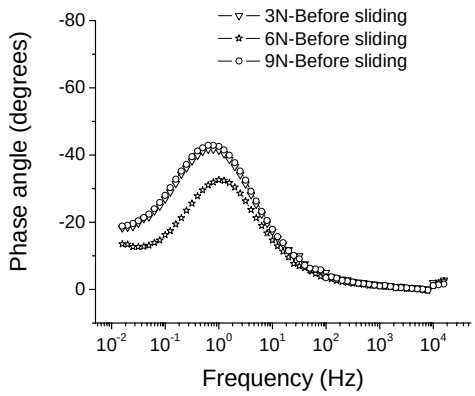

(a) Bode phase plot before sliding , 0.0 V

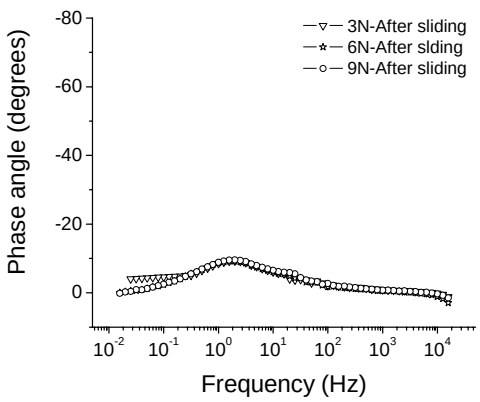

(b) Bode phase plot after sliding , 0.0 V

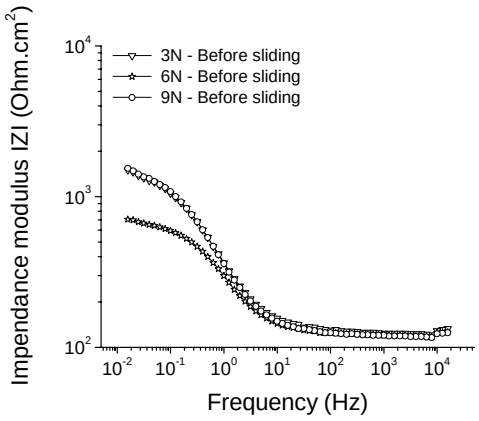

(c) Bode impedance |Z| plot before sliding, 0.0 V

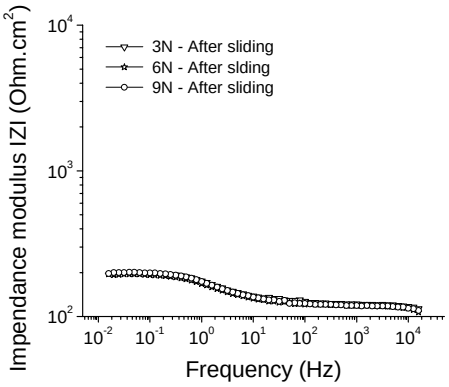

(d) Bode impedance |Z| plot after sliding, 0.0 V

Figure 9 (a-d) Bode phase plot (Frequency vs. Phase angle) and Bode Z plot (Frequency vs. Impedance modulus |Z|) obtained in TiC_xO_y film before and after sliding at 3, 6 and 9 N constant potential of 0.0 V

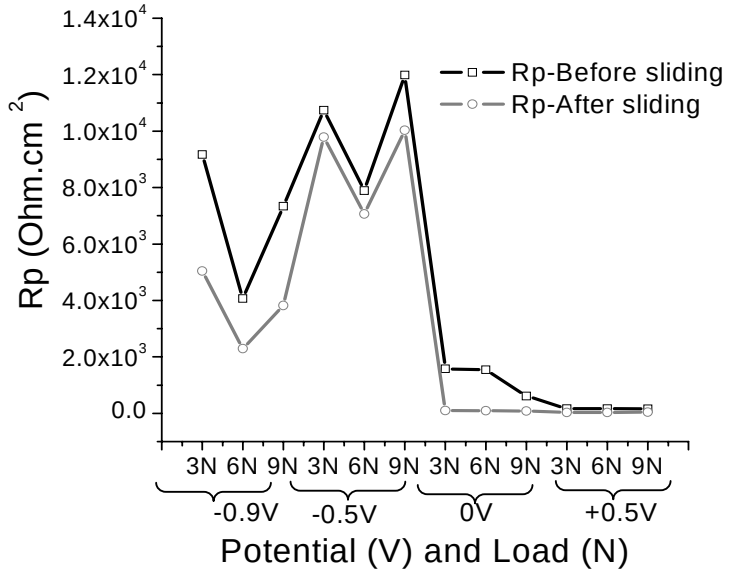

Figure 10 Variation of Polarization resistance (R_p) as a function of load and potential

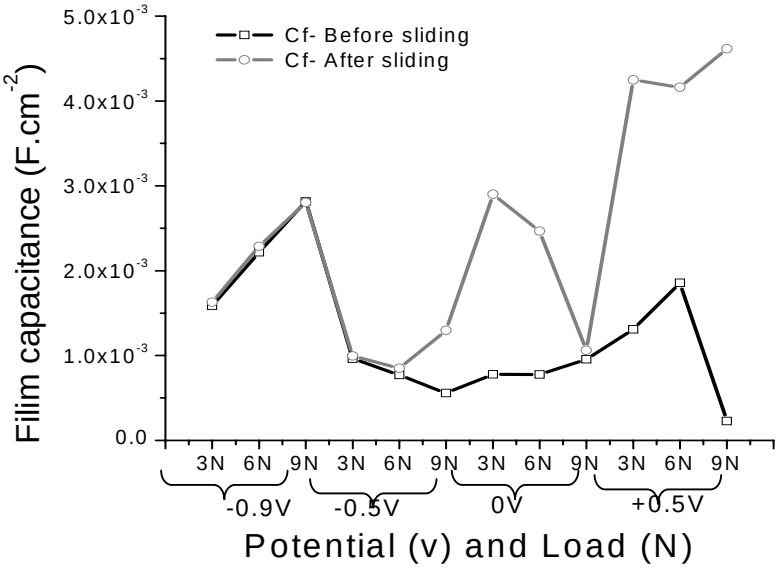

Figure 11 Variation of film capacitance (C_f) as a function of load and potential

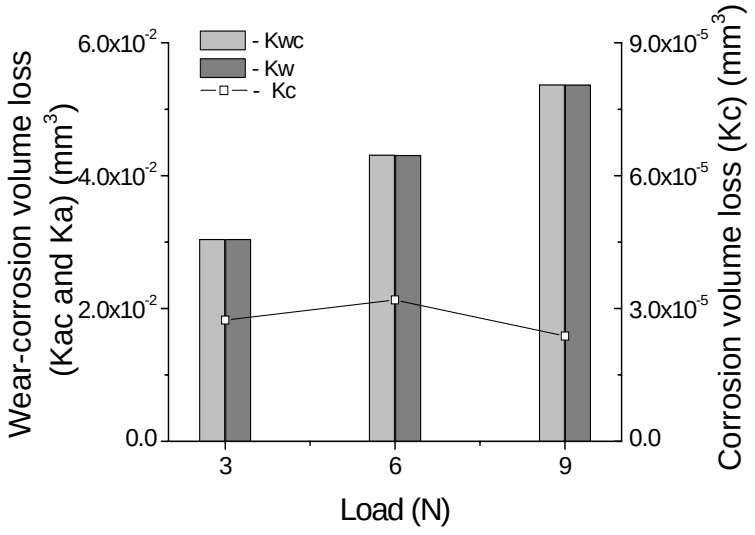

(a) Variation of K_{wc}, K_w and K_c,-0.5 V

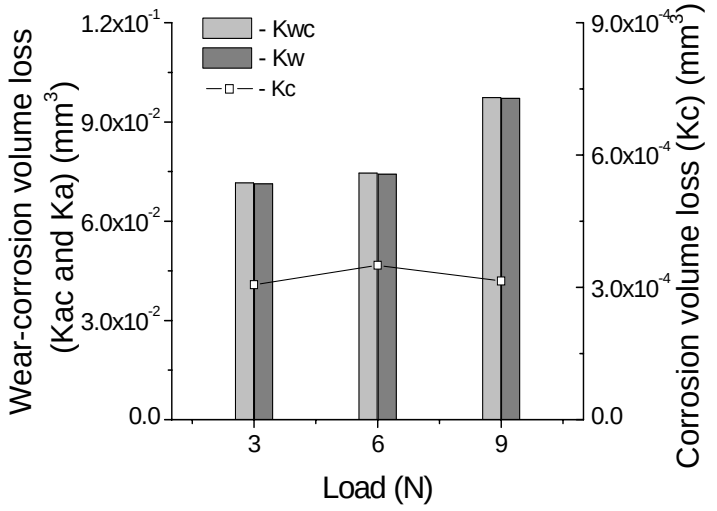

(b) Variation of K_{wc}, K_w and K_c , at 0 V

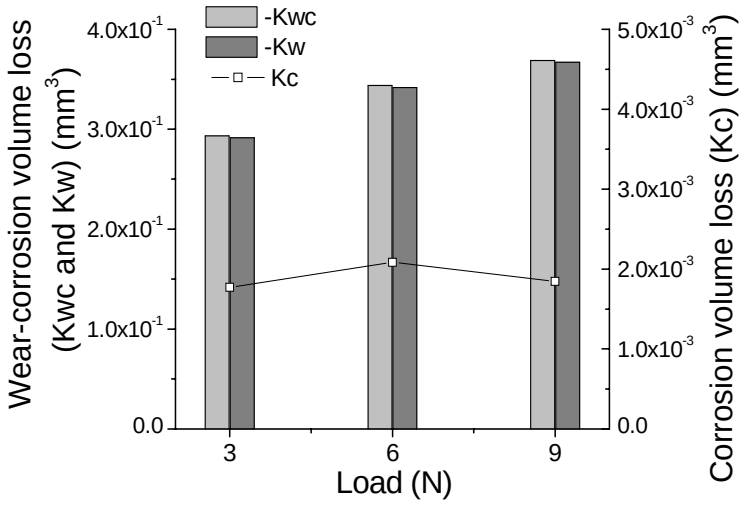

(c) Variation of K_{wc}, K_w and K_c, at +0.5 V

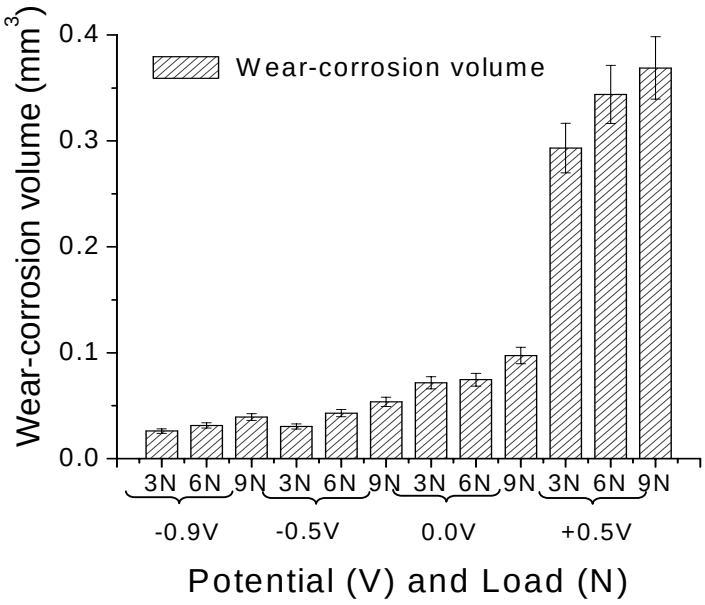

(d) Variation of (K_{wc}): all the results in one scale

Figure 12 (a-d) Variation of wear-corrosion volume loss (K_{wc}) and corrosion volume loss at selected potentials

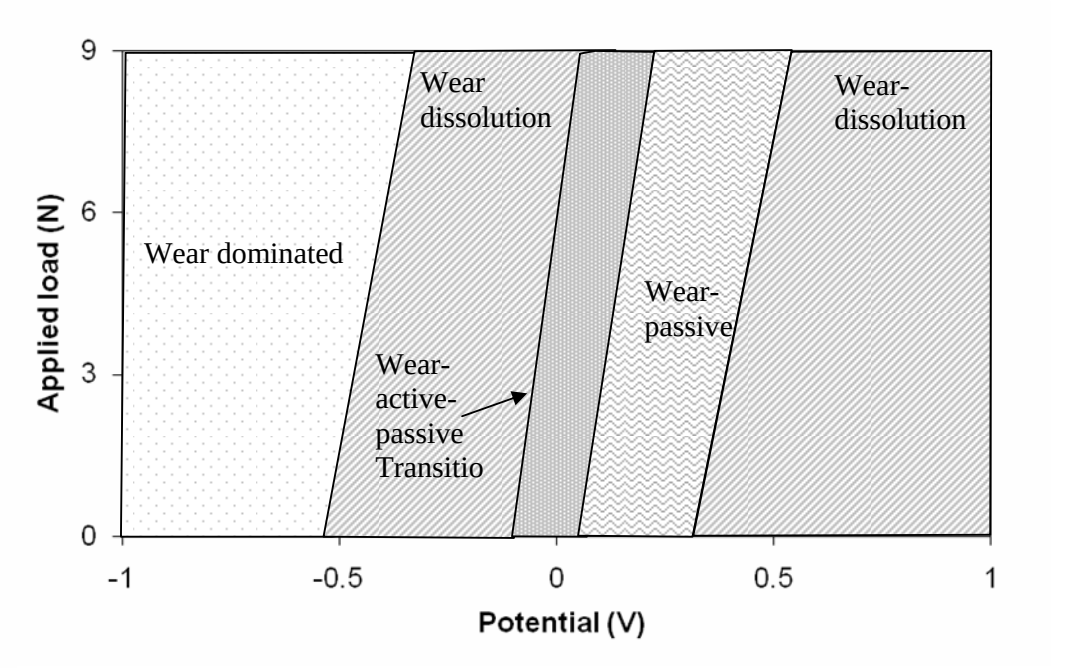

Figure 13 Tribocorrosion mechanisms map as a function of applied potential and load

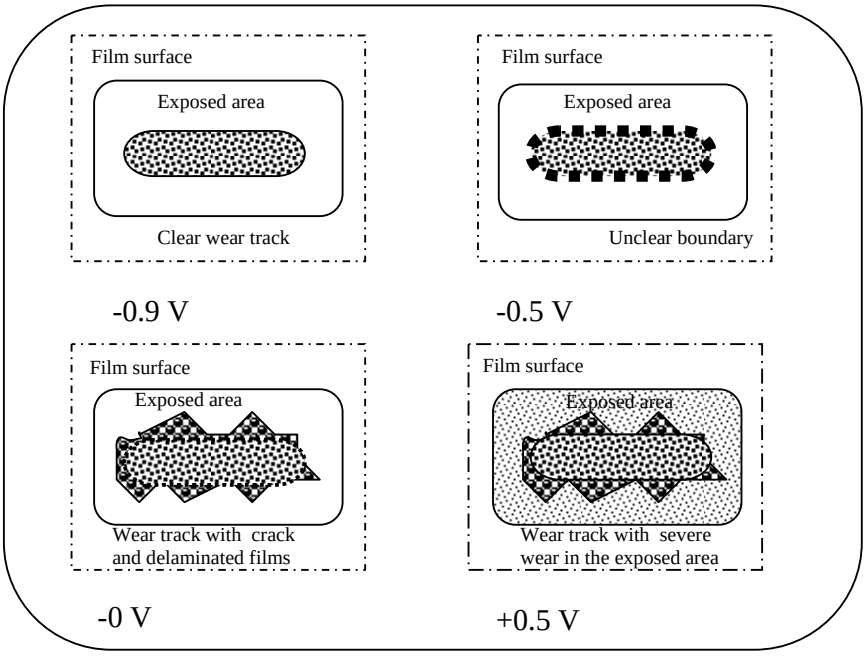

Figure 14 Schematics diagram showing surface changes after the tribocorrosion test, showing the effect of increasing applied potential

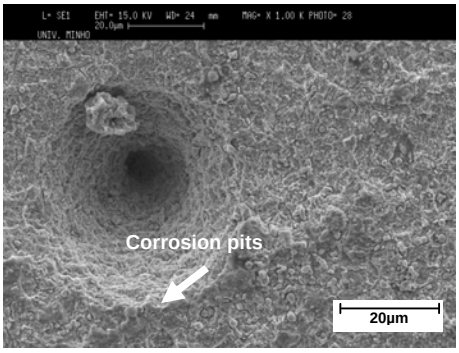

(a) Pits, +0.5 V, 3N

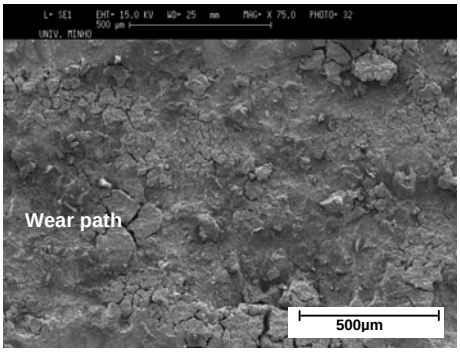

(b) Cracks and +0.5 V, 3N

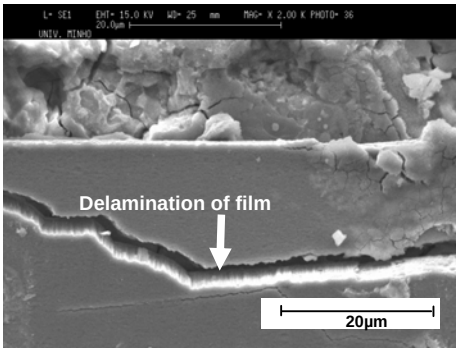

(c) Dissolution of the substrate +0.5 V, 3N

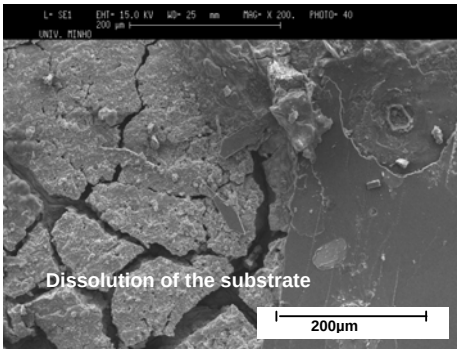

(d) Film is completely removed, 0 V, 6N

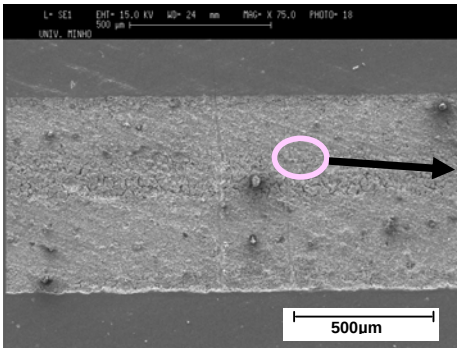

(e) Clear wear path

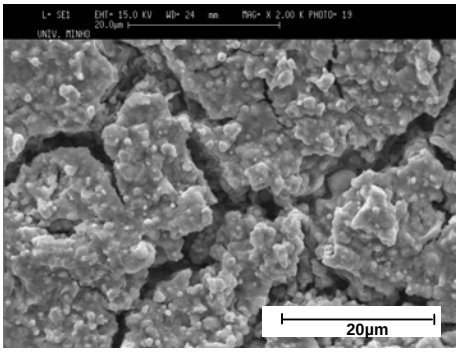

(f) Enlarged view of the worn surface (e)

Figure 15 (a-f) SEM images of the worn surfaces, after the tribocorrosion exposure

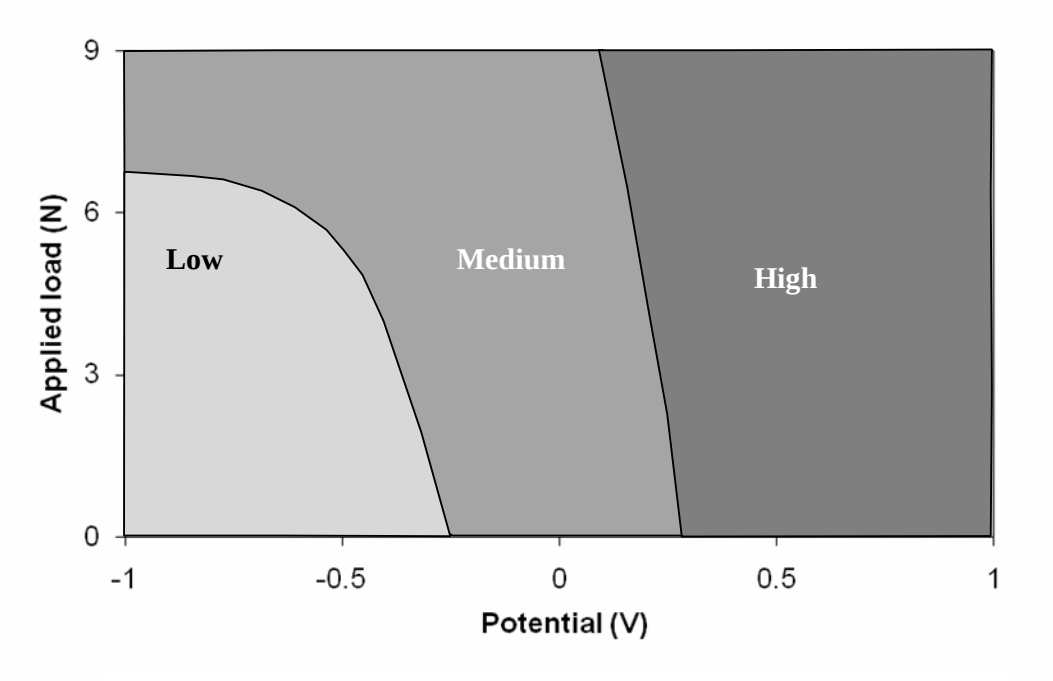

Figure 16 Wastage map as function of applied potential ad load

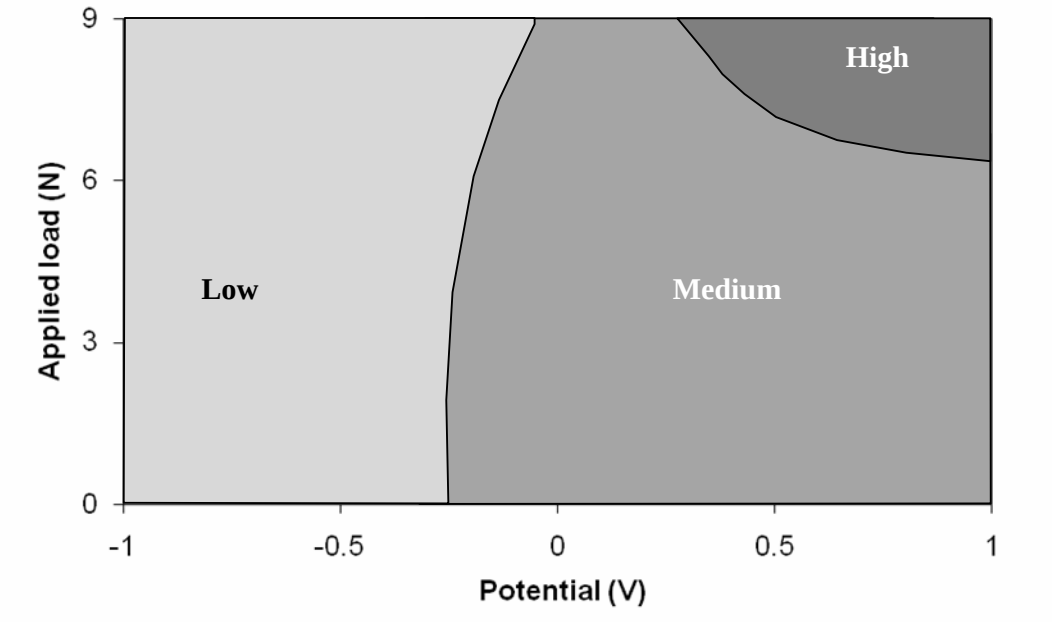

Figure 17 Synergism map as a function of applied potential and load